TECHNICAL REPORTS

nature medicine

In vivo imaging of axonal degeneration and regeneration in the injured spinal cord

Martin Kerschensteiner[1,2], Martin E Schwab[2], Jeff W Lichtman[1] & Thomas Misgeld[1]

The poor response of central axons to transection underlies the bleak prognosis following spinal cord injury. Here, we monitor individual fluorescent axons in the spinal cords of living transgenic mice over several days after spinal injury. We find that within 30 min after trauma, axons die back hundreds of micrometers. This acute form of axonal degeneration is similar in mechanism to the more delayed Wallerian degeneration of the disconnected distal axon, but acute degeneration affects the proximal and distal axon ends equally. *In vivo* imaging further shows that many axons attempt regeneration within 6–24 h after lesion. This growth response, although robust, seems to fail as a result of the inability of axons to navigate in the proper direction. These results suggest that time-lapse imaging of spinal cord injury may provide a powerful analytical tool for assessing the pathogenesis of spinal cord injury and for evaluating therapies that enhance regeneration.

After spinal cord injury, axons are known to undergo a series of changes: proximal axon ends 'die back' and do not regenerate, whereas distal axon ends undergo Wallerian degeneration[1]. Despite much effort, the axonal biology underlying these events is poorly understood, mainly because axons in the mammalian central nervous system (CNS) elude direct observation. Without knowledge of an axon's dynamic behavior, the intertwined processes of axon degeneration and regeneration might be hard to untangle. Furthermore, the lack of direct *in vivo* observation impedes the evaluation of therapeutic interventions. For example, with conventional tracing techniques and postmortem analysis, it is difficult to differentiate regenerating fibers that were induced by a therapeutic intervention from either compensatory sprouting of undamaged fibers or from 'spared' fibers that persisted at the lesion site[2].

To overcome these limitations we have developed an approach that allows direct observation of individual axons over long distances (millimeters) and periods of time (days) with high spatial (sub-micron) and temporal (seconds) resolution. Using this technique, we describe a novel form of symmetrical post-traumatic degeneration underlying axonal dieback, characterize the *in vivo* time course of Wallerian degeneration, and provide the first time-lapse recordings of axonal regeneration in the CNS. Based on these results, we believe that *in vivo* imaging holds great promise for assessing experimental therapies for spinal cord injury and other white matter pathologies.

RESULTS

In vivo imaging of single sensory axons in the spinal cord

To visualize individual axons in the spinal cord of living mice we used a transgenic mouse line (GFP-S mice), in which a neuron-specific fragment of the *Thy1* promoter drives cytoplasmic expression of high levels of green fluorescent protein (GFP) in subsets of neurons, including sensory neurons in the dorsal root ganglia (DRG; **Fig. 1**)[3]. These DRG neurons give rise to large myelinated axons, which run superficially within the dorsal column of the spinal cord (**Fig. 1a**) and are commonly studied to assess regeneration in the mammalian CNS[4,5].

We modified a laminectomy procedure to allow lowering a 'dipping-cone' water immersion objective onto the dorsal spinal cord (**Fig. 1b**,**e**) and used computer-assisted wide-field microscopy[6] to visualize DRG axons *in vivo* over several spinal segments (**Fig. 1f**). Subcellular details such as nodes of Ranvier or gray matter collaterals were easily visible and could be directly correlated with postmortem reconstructions (**Fig. 2** and **Supplementary Fig. 1** online).

Repetitive imaging of axonal changes following injury

After documenting the morphology of a GFP-labeled axon and its position in relation to nearby blood vessels by fluorescence microscopy, the animal was transferred to a dissection microscope. We then selectively transected the labeled axon (and a bundle of surrounding unlabeled axons) with a small pin (diameter, 200 µm) mounted on a micromanipulator, using the blood vessels as fiduciary marks (**Fig. 1g**).

Under the fluorescence microscope, we saw a gap in the continuity of the axon, caused by the direct impact of the needle (removing each axon end ~100 µm from the lesion center). By 24–30 h, when we first reimaged the axons, both axon ends had died back symmetrically (**Fig. 2a**). This dieback moved the axon ends on average 307 ± 75 µm further away from the original lesion border ($n = 10$). On many axon

[1]Department of Molecular and Cellular Biology, Harvard University, 7 Divinity Avenue, Cambridge, Massachusetts 02138, USA. [2]Department of Neuromorphology, Brain Research Institute, Department of Biology, ETH and University of Zurich, Winterthurer Strasse 190, CH-8057, Zurich, Switzerland. Correspondence should be addressed to T.M. (tmisgeld@mcb.harvard.edu).

Published online 10 April 2005; doi:10/nm1229

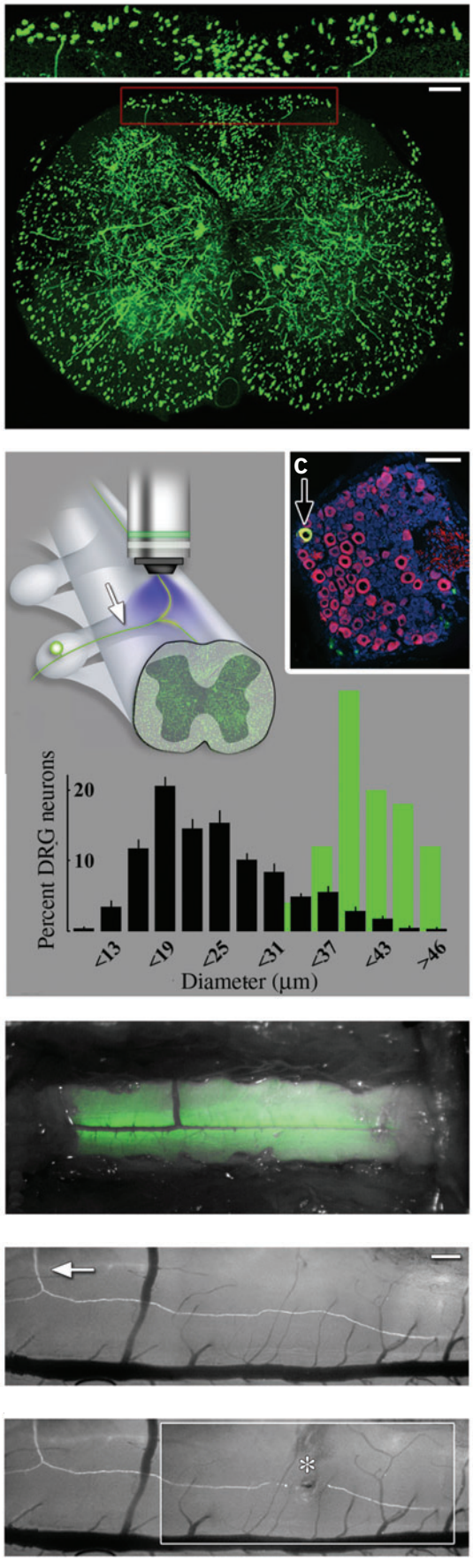

Figure 1 Fluorescent labeling of sensory DRG axons in GFP-S mice. (**a**) Cross-section of the spinal cord of a GFP-S mouse with a subset of GFP-labeled axons. The red box (enlarged ×2 above) delineates the superficial dorsal funiculus where sensory axons can be imaged *in vivo*. (**b**) Schematic representation of the *in vivo* imaging approach (arrow, entry of a DRG axon through the dorsal root). (**c**) Cross-section of a GFP-S DRG stained for neurofilament (red) and a Nissl-like stain (blue). In the GFP-S line, most DRGs contain no or only one labeled neuron. On this section a single GFP-positive neuron (arrow; GFP in green) can be seen, which also stains for neurofilament (and thus appears yellow). (**d**) Size distribution of GFP-labeled DRG neurons (green bars, $n = 50$ cells) superimposed on the entire DRG neuron population (black bars; based on Nissl-like stain, $n = 1{,}000$). GFP labels only large DRG neurons (average diameter 40.92 ± 0.61 μm), which are also immunoreactive for neurofilament (**c**; and data not shown). (**e**) View of the dorsal spinal cord of a GFP-S mouse exposed by a laminectomy of the vertebrae C3–C6. The GFP fluorescence (green) is superimposed on a black-and-white image of the spinal cord (vessels appear black). (**f**) A single GFP-labeled DRG axon (imaged *in vivo)* extends over several spinal segments. DRG axons can be identified by entry into the spinal cord through a dorsal root (arrow) and branching into a short descending (left) and a long ascending branch (right). (**g**) The axon in **f** is shown after transection with a small pin (asterisk). Scale bars in **a** and **f**, 200 μm and in **c**, 100 μm.

tips bulb-like structures had formed (58.8%; 10 of 17 axons), which often showed shape changes from day to day (**Fig. 2b**)[7]. During the next 24 h, the proximal end shortened only slightly more (31.8 ± 10.5 μm, $n = 5$).

Acute axonal degeneration occurs minutes after trauma

The temporal and spatial characteristics of axonal dieback, as well as its cellular mechanism, are unclear, with evidence supporting either retraction or fragmentation[1,8–10]. We therefore set out to clarify the mechanism of axonal dieback by imaging axons at ~1 frame per minute during the first hours after lesion. Axon ends were initially stable for 10–20 min but then underwent sudden fragmentation, a process we have termed 'acute axonal degeneration' (AAD; **Fig. 3a**,**b** and **Supplementary Movie 1** online). AAD lasted less than 5 min and extended over 200–300 μm, thereby accounting for 89 ± 2% of all axon loss between 2 min and 4 h after lesion ($n = 15$; **Fig. 3b**,**c** and **Supplementary Movie 2** online). It affected distal and proximal axon ends almost identically (**Fig. 3c**). Thus, in contrast to Wallerian degeneration, AAD removes axon segments that are still connected to the soma and could lead to secondary denervation by affecting side branches that bear synaptic contacts. Indeed, when we placed the lesion in proximity to major branch points (for example, the first bifurcation near their entry point into the dorsal column), AAD spread beyond the branch point in 40% of axons and thus resulted in disconnection of the unlesioned branch from the soma (6 of 15 axons). After AAD was completed, a different process (slow axonal retraction) ensued, which accounted for the remaining dieback and resulted in bulb formation on most axon ends (**Fig. 3d**, **Supplementary Movie 3** and **Supplementary Fig. 2** online).

After about 30 h, the fates of the proximal and the distal cut axon ends sharply diverged. Whereas the proximal end remained stable (or showed signs of early outgrowth), the distal end suddenly began to rapidly fragment owing to Wallerian degeneration (**Fig. 2c** and **Supplementary Movie 4** online). The onset of Wallerian degeneration was asynchronous both between axons (some of which persisted for up to 48 h; **Fig. 2b**) and even within the same axon arbor, where two sister branches that were lesioned synchronously sometimes persisted for different periods of time. In most cases, when we imaged axons undergoing Wallerian degeneration with high time resolution,

we found that fragmentation started near the tip of the transected axon end and spread in a proximal to distal direction ($n = 3$; **Fig. 2c**). Confocal reconstructions of axons, which were imaged while undergoing Wallerian degeneration and fixed immediately, showed an ordered sequence of changes starting with the formation of swellings ('beading'), the connections of which became progressively thinner until the fragments finally separated (**Supplementary Fig. 1** online).

AAD shares mechanisms with Wallerian degeneration

AAD is clearly distinct from Wallerian degeneration in terms of where and when it occurs. But many of the morphological characteristics of both forms of post-traumatic degeneration were indistinguishable. These include, for example, the speed of fragmentation once initiated (at least 70 µm/min for both AAD and Wallerian degeneration), the size of fragments (AAD: 17 ± 1 µm, $n = 58$, versus WD: 20 ± 1 µm, $n = 61$) and their spacing (AAD: 28 ± 2 µm, $n = 49$, versus WD: 35 ± 2 µm, $n = 58$). We tested whether these similarities were indicative of a common molecular mechanism. First, we used a spontaneous dominant mutation in C57/BL6 mice known as 'Wallerian degeneration slow' (WLD-S), which substantially delays Wallerian degeneration[11,12]. AAD was also largely absent in WLD-SxGFP-S crosses (**Fig. 3e**, **Supplementary Fig. 2** and **Supplementary Movies 5** and **6** online). Slow axonal retraction, though, was unaffected by the WLD-S mutation (**Supplementary Fig. 2** and **Supplementary Movie 7** online). Second, calpain proteases, which are key mediators of cytoskeletal degradation during Wallerian degeneration[13,14], are also involved in AAD. An antibody, which specifically recognizes fragments of calpain-mediated spectrin proteolysis[15], showed strong immunoreactivity spanning 400 µm from both lesion borders around the peak of AAD (30 min after lesion), but not before the onset of AAD (5 min; **Supplementary Fig. 3** online). The presence of calpain inhibitors resulted in a complete block of AAD *in vivo* (**Fig. 3e** and **Supplementary Fig. 3** online).

Many axons start regenerating within 24 h after lesion

The proximal ends of most transected axons stabilized about 300 µm from the lesion site, where they persisted for the remaining observation period (3–7 d). Almost 30% of these proximal ends (29.4%; 5 of 17 axons) started growing during the first 2 d after lesion. The earliest sprouts formed 6–24 h after lesion, much earlier than described previously (**Fig. 4**)[16,17]. Sprouts occurred in two forms: 'terminal sprouts' at the tips of transected axons (**Fig. 4c** and **Supplementary Fig. 4** online), and 'nodal sprouts' at a proximal node of Ranvier (**Supplementary Fig. 5** online). The speed of this initial growth was at least 4.3 ± 0.6 µm/h ($n = 4$), which is roughly 30% of the growth speed measured for regenerating axons in the peripheral nervous system (PNS) 1 d after lesion (~0.3 mm/d)[18]. Repetitive imaging of the same axon allowed us to follow the growth of individual axons over several days. Some axons seemed to grow fast and unbranched, whereas others grew more slowly and formed numerous side branches. In some axons, both forms of growth occurred in sequence. For example, the most advanced tip of the axonal sprout shown in **Figure 4** initially grew fast and in a straight trajectory (average speed of 4.3 µm/h during the first 48 h), but slowed down to about 0.7 µm/h thereafter, when profuse branches formed. But if all side branches were combined, the overall growth rate remained largely unchanged (5.7 µm/h between 48 and 72 h). This is in contrast to peripheral axons, which continue to grow in a straight trajectory and speed up their growth threefold during the 3 d after lesion[18]. After fixation, growing axons could be reconstructed in detail by confocal microscopy (**Fig. 4** and **Supplementary Fig. 5** online) and traced back to their neuronal soma in the DRG (**Supplementary Fig. 4** online). Confocal reconstructions of the axon shown in **Figure 4** revealed that the parts of the axon that formed during different phases of growth showed a specific morphology: the segment that formed during fast growth within the first 2 d after transection had a more regular appearance and a caliber close to that of the transected parental axon (**Fig. 4c**). In contrast, thin, irregular axon segments, which resembled growth cones because they were spiked by numerous small filopodia, formed between 2 and 3 d after transection (**Fig. 4c**). Irrespective of speed or pattern of growth, lesioned axons seemed to lack directional information: none managed to grow back to (or beyond) the lesion site (even though they grew on average >150 µm already within the first 48 h after lesion, and large sprouts can extend for >1 mm at 14 d after lesion). Rather, they grew laterally or even in a 'U turn', which accounts for the large axon convolutes that we observed 1–2 weeks after injury.

DISCUSSION

It was recognized decades ago that after transection axonal loss exceeded what could simply be explained by traumatic impact, suggesting that axons must die back from the lesion site[1]. We now show

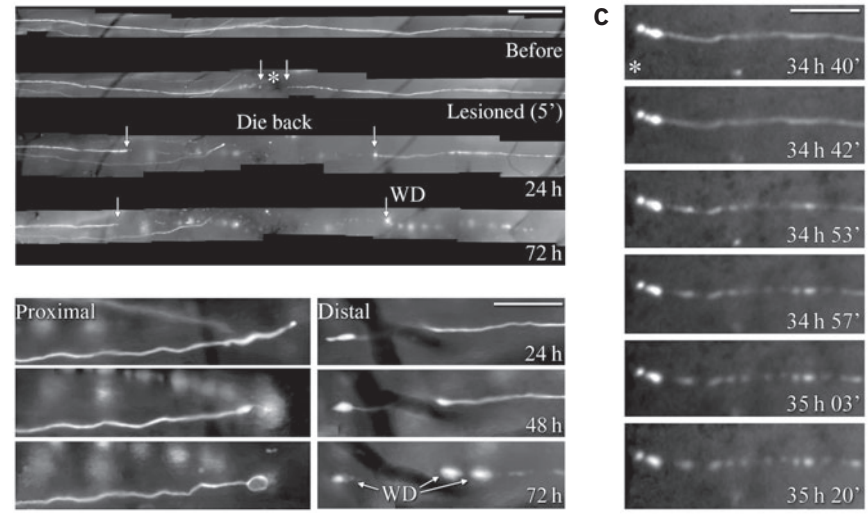

Figure 2 Repetitive *in vivo* imaging of DRG axons after spinal cord injury. (**a**) Changes in an ascending DRG axon branch *in vivo* during the first 72 h after lesion, including dieback and Wallerian degeneration (WD; imaged before, at 5 min, 24 h and 72 h after lesion). Asterisk, lesion; white arrows, axonal tips. Left, proximal; right, distal. The dark area near the lesion is a small hemorrhage. Scale bar, 250 µm. (**b**) Detailed view of proximal and distal axon ends of another axon after lesion, illustrating bulb formation (proximal and distal) and Wallerian degeneration (distal; arrows at 72 h). Scale bar, 100 µm. (**c**) Time series of a distal axon end undergoing Wallerian degeneration 34–35 h after mechanical transection (**Supplementary Movie 4** online). After an initial phase of stability (upper 2 frames) the axon undergoes sudden fragmentation, which spreads rapidly away from the tip (lower 4 frames). A confocal reconstruction of a large stretch of this axon is presented in **Supplementary Figure 1** online. Scale bar, 100 µm.

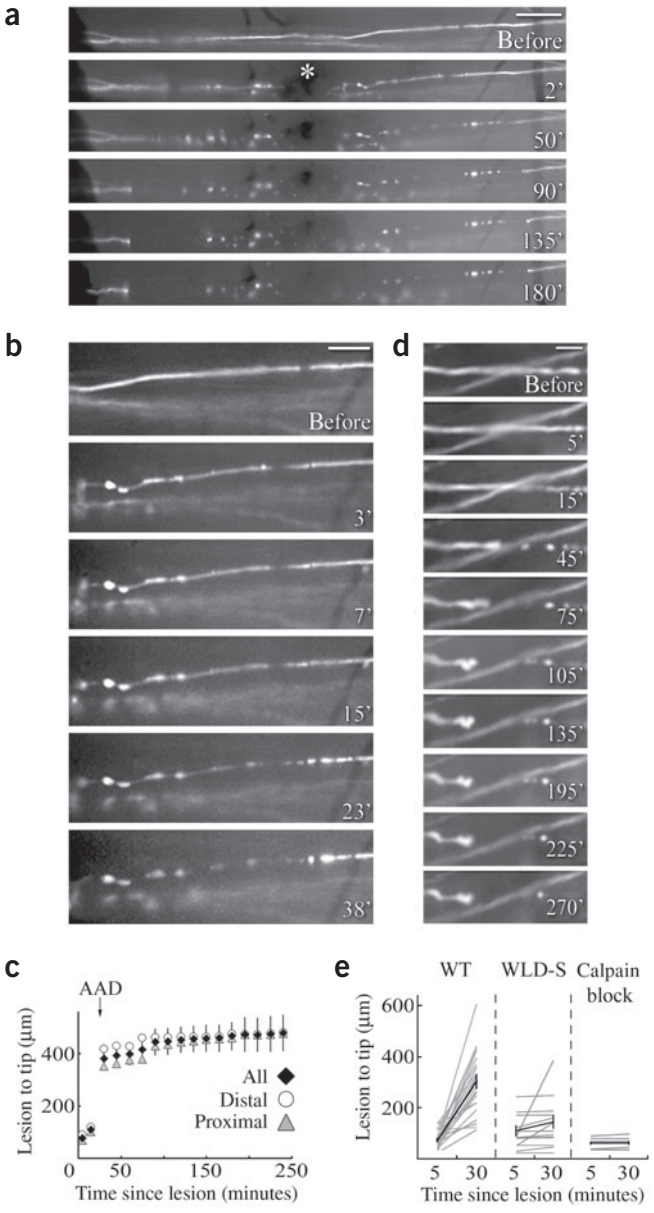

Figure 3 Imaging acute axonal degeneration *in vivo*. (**a**) *In vivo* time-lapse imaging of an axon for 180 min after lesion (marked by asterisk; **Supplementary Movie 1** online). An initial lag phase (2 min) is followed by AAD (50 min) and later slow axonal retraction. Axonal bulbs form on both ends of the transected axon (last three frames). Scale bar, 100 µm. (**b**) Higher temporal resolution (about 1 min per frame) of axon end to the right in **a** undergoing AAD (**Supplementary Movie 2** online). Scale bar, 50 µm. (**c**) Quantification showing that most of the axon loss during the first 4 h after lesion is the result of AAD (arrow; the process takes less than 5 min; data not shown). The extent of axonal loss is similar in proximal ($n = 5$–6) and distal ($n = 3$–5) axon ends (mean ± s.e.m.). (**d**) Proximal end of an additional DRG axon imaged for 270 min after lesion. The image series shows axonal fragmentation (15–45 min) followed by retraction and bulb formation (45–270 min; lesion is to the right outside the frame; **Supplementary Movie 3** online). Scale bar, 25 µm. (**e**) Quantification of AAD in individual axon ends. Each line represents a single axon end at 5 and 30 min after lesion, the black line shows the mean of all axon ends (± s.e.m.). In wild-type animals (left) axonal loss was 230 ± 28 µm between 5 and 30 min after lesion for all axon ends ($n = 22$; proximal ends, 197 ± 28 µm versus distal ends, 269 ± 51 µm). In contrast, AAD is substantially decreased in WLD-S mice (middle; fragmentation between 5 and 30 min after lesion in WLD-SxGFP-S mice: 34 ± 21 µm, $n = 14$, versus C57/BL6xGFP-S control mice: 200 ± 37 µm; $P < 0.001$). For *in vivo* time-lapse see **Supplementary Fig. 2** and **Supplementary Movies 5** and **6** online. AAD is completely abolished in wild-type mice in the presence of calpain inhibitors (right; fragmentation between 5 and 30 min after lesion after calpain block: 1 ± 1 µm, $n = 10$, versus control mice treated with carrier solution: 197 ± 61 µm; $P < 0.001$). For *in vivo* time-lapse see **Supplementary Fig. 3** online.

that most early axonal dieback occurs by AAD, a fast, regulated process of fragmentation that accounts for the majority of secondary axonal loss during the first days after trauma. Notably, AAD shares morphological and mechanistic features with Wallerian degeneration, the paradigmatic case of post-traumatic axon degeneration. This suggests that these distinct forms of axonal degeneration activate a common cellular program of axonal 'self-destruction'[19]. Beyond explaining dieback, AAD (in contrast to Wallerian degeneration) is potentially of considerable clinical relevance as it augments denervation by removing spared side branches of axons proximal to the lesion. AAD can also impede axonal regeneration, as axons have to cover a longer distance to reach the lesion site where a glial scar may have had more time to become an obstruction.

Our observations of growing axons suggest a scenario in which axon regeneration fails mainly as the result of an axon's inability to grow back along its original trajectory. Notably, many axons (about 30%) mount an initial growth response, some between 6 to 24 h after lesion. During this early growth phase, axons seem to grow in two different 'modes': elongation, in which the axons advance fast and straight, and branching, in which numerous small lateral outgrowths form. Branching seems to be initiated when elongation stalls (or when it is quenched from the beginning) to allow the axon to navigate outside pre-established axon pathways and can, for example, contribute to the formation of 'detour' pathways[20]. Neither mode of growth, however, allows axons to advance substantially closer to their original targets. Their erratic growth pattern suggests that this is at least partly the result of a lack of directional information needed to reiterate the original growth trajectory (which is available to their PNS counterparts)[21].

Besides the description of pathological processes, *in vivo* microscopy can also be used to monitor the efficacy and mechanism of therapeutic interventions designed to prevent degeneration or to promote regeneration, as illustrated by the use of calpain inhibitors to block AAD. *In vivo* imaging can overcome many of the limitations of conventional tracing methods, because (i) transection can be directly confirmed, (ii) nonmonotonous behavior (such as dieback followed by outgrowth) can be resolved down to time intervals of a few seconds, and (iii) mechanistic insight can be inferred from time-resolved observations.

More generally, how axons respond to injury is not only relevant to spinal cord trauma but to numerous other white matter pathologies, such as multiple sclerosis and amyotrophic lateral sclerosis, to which this technique can be easily adapted.

METHODS

Mice. Adult transgenic GFP-S mice (2–12 months of age) were used[3]. The distribution of fluorescent proteins in *Thy1* mice closely reflects the morphological and ultrastructural changes axons undergo during degeneration[22]. We confirmed by immunostaining that GFP colocalized with a cytoskeletal axonal protein, neurofilament, and thus that axons lost continuity rather than merely redistributing their cytoplasm during apparent fragmentation (**Supplementary Fig. 6** online).C57/BL6 mice, homozygous for the dominant WLD-S mutation[11] (Harlan), were crossed with GFP-S mice to obtain heterozygous WLD-SxGFP-S mice, which were used between 2 and

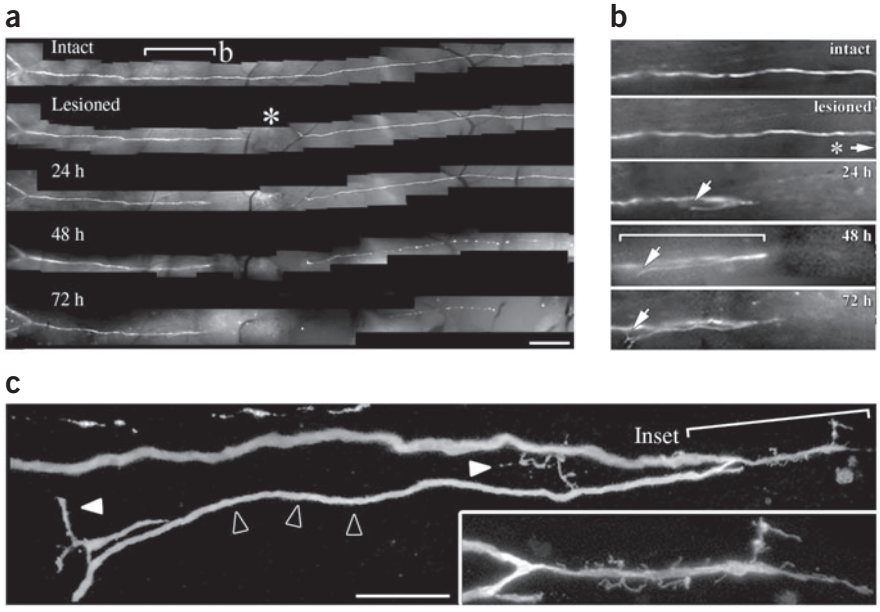

Figure 4 Monitoring early axonal outgrowth *in vivo*. (**a**) *In vivo* time-lapse series of an axon in the spinal cord of a GFP-S mouse imaged before and four times on consecutive days after lesion (asterisk). Scale bar, 250 µm. Bracket braces area magnified in **b**. (**b**) High-power view of the growing axon tip (arrow). Image is magnified fourfold from **a**. The earliest attempts of axonal outgrowth are already evident 24 h after transection. The growing axon tip seems to lack directional information, as it extends away from the lesion site and its original targets. Bracketed area is shown in **c** after fixation. (**c**) Confocal reconstruction of the growing axon tip in **b** at 72 h. Scale bar, 25 µm. Some segments of the axon have an almost normal appearance and caliber (open arrowheads), whereas side branches are fine and irregular (solid white arrowheads). The straight segments formed during initial fast elongation (in **b**; 0–48 h). This initial elongation stalls and is followed by formation of side branches (48–72 h). Inset shows a side branch of the growing axon with numerous filopodia. Image is magnified twofold from **c**.

4 months to avoid age-dependent weakening of the WLD-S phenotype[23]. Age-matched controls were GFP-S mice bred with wild-type C57/BL6-mice (Jackson Laboratory; C57/BL6xGFP-S mice).

Surgery. Mice were anesthetized with ketamine-xylazine (ketamine 87 mg/kg, xylazine 13 mg/kg intraperitoneally). Ketamine-xylazine was reapplied subcutaneously every 60 min. Animals were intubated, ventilated, the laminae covering cervical segments 3 to 6 were removed and the dura was opened locally. Body temperature was controlled by a heated pad (37 °C). For recovery, the spinal cord was covered with a dura substitute (W. L. Gore & Associates) and the laminectomy was closed. The animals were injected with atipamezole (1 mg/kg intraperitoneally), placed in a heated recovery chamber, and buprenorphine (0.1 mg/kg, subcutaneously) was injected daily for analgesia. For reimaging, the procedure was repeated up to five times. All procedures were approved by the Animal Studies Committees of Washington University, St. Louis, Missouri and Harvard University, Cambridge, Massachusetts.

Transection of CNS axons. To transect individual identified axons, a thin needle (diameter 200 µm; Fine Science Tools), mounted on a micropositioner (Narishige), was used to lesion pre-selected axons that crossed identifiable blood vessels. For some long-term, time-lapse experiments or for postmortem examination of fixed tissue a hand-held 32-gauge hypodermic needle or a pair of fine iridectomy scissors (Fine Science Tools) was used to transect axons.

***In vivo* time-lapse imaging.** We used an Olympus BX51 microscope equipped with ×4/0.13 dry and ×20/0.5 dipping cone water-immersion objectives (Olympus), an electronic shutter (Sutter Instruments) and a *z*-stepper (Ludl Electronic Products) controlled by MetaMorph software (Universal Imaging). Preheated (33–35 °C near the field of imaging) lactated Ringer's or artificial mouse cerebrospinal fluid was used to superfuse the spinal cord. We acquired streams of 25 images (50 ms exposure) while the ventilator was turned off to prevent respiration artifacts. Image stacks were then aligned to remove heartbeat using Autoquant (Autoquant Imaging) or custom-written software. In-focus planes were selected, stacks of aligned, in-focus frames averaged, and montaged to overviews in Photoshop (Adobe). Three hours of continuous illumination of the same intensity as used in the *in vivo* experiments did not change axon morphology, ruling out substantial phototoxicity.

Quantification of axonal changes. Using MetaMorph software, we measured the distance of the last piece of the axon end that appeared connected (the axon 'tip') to the lesion center, fragment lengths, as well as fragment distance (distance between the centers of two neighboring fragments) after AAD or Wallerian degeneration. We measured regeneration as the change in distance of the most advanced axon tip in relation to fixed landmarks (for example, blood vessels or the parental axon arbor).

Immunohistochemistry. Spinal cords were fixed with 4% paraformaldehyde in phosphate-buffered saline (PBS) for 12–24 h. Vibratome sections (50–200 µm) were imaged directly, or post-fixed in methanol (–20 °C, 15 min) before blocking in 'staining buffer' (PBS, 2.5–5% bovine serum albumin, 1–2% goat serum, 0.2–1% Triton X-100). Antibodies were diluted in the same buffer (anti-spectrin degradation product, 1:500, gift of T.C. Saido, RIKEN Brain Science Institute, Japan; anti-neurofilament 150, 1:1,000, Chemicon; secondary antibody donkey-anti-rabbit Cy3, 1:2000, Jackson ImmunoResearch). Sections were mounted in Vectashield (Vector Laboratories). Size distributions were determined from cryosectioned GFP-S DRGs stained with a far-red Nissl-like stain (NeuroTrace Far Red; Molecular Probes). Calpain-mediated spectrin proteolysis was quantified blinded using projected confocal stacks ($n = 15$ sections from 3 animals) by counting immunopositive axonal fragments (disconnected spherical profiles) 100, 200, 300 and 400 µm from the lesion border.

Confocal imaging. We obtained confocal images on a Biorad MRC1024 confocal system on a BX50 microscope (using a ×40/1.15 water or a ×60/1.4 oil immersion objective; Olympus).

Pharmacological manipulation *in vivo*. Calpain proteases were inhibited using EST (irreversible; Calbiochem) and calpain inhibitor III (CI III; reversible; Calbiochem) at 100 µmol/L each during 20 min of preincubation. After lesion, we imaged for 1 h using perfusate containing 100 µmol/l CI III. Blockade using a commercially available calpain inhibitor mix (Calbiochem) yielded identical results. Controls were done with equal concentrations of carrier (DMSO for EST and ethanol for CI III). Calpain inhibition was confirmed by immunostaining (**Supplementary Fig. 3** online).

Statistical analysis. Results are given as mean ± s.e.m. Statistical significance ($P < 0.05$) was determined using unpaired *t*-tests in Prism software (GraphPad).

Note: Supplementary information is available on the Nature Medicine website.

ACKNOWLEDGMENTS
The authors wish to thank J. Sanes for providing GFP-S mice and support, T.C. Saido for providing the antibody specific for spectrin degradation products, J. Tollett for animal husbandry, J. Lu for writing software, L. Godinho, F. Bareyre and J. Sanes for suggestions and critical reading of the manuscript. This work was supported by grants from the Christopher Reeve Paralysis Foundation (T.M.), the Emmy Noether Program of the Deutsche Forschungsgemeinschaft (T.M.,

M.K.) and grants from the Swiss National Science Foundation (M.E.S.) and the US National Institutes of Health (J.W.L.).

COMPETING INTERESTS STATEMENT

The authors declare that they have no competing financial interests.

Received 11 November 2004; accepted 2 January 2005
Published online at http://www.nature.com/naturemedicine/

1. Ramón y Cajal, S. *Degeneration and regeneration of white matter in Cajal's Degeration and Regeneration of the Nervous System* (eds DeFelipe, J. & Jones, E.G.) ch.4 (Oxford Univ. Press, New York, 1991).
2. Steward, O., Zheng, B. & Tessier-Lavigne, M. False resurrections: distinguishing regenerated from spared axons in the injured central nervous system. *J. Comp. Neurol.* **459**, 1–8 (2003).
3. Feng, G. *et al.* Imaging neuronal subsets in transgenic mice expressing multiple spectral variants of GFP. *Neuron* **28**, 41–51 (2000).
4. Neumann, S. & Woolf, C.J. Regeneration of dorsal column fibers into and beyond the lesion site following adult spinal cord injury. *Neuron* **23**, 83–91 (1999).
5. Qiu, J. *et al.* Spinal axon regeneration induced by elevation of cyclic AMP. *Neuron* **34**, 895–903 (2002).
6. Walsh, M.K. & Lichtman, J.W. *In vivo* time-lapse imaging of synaptic takeover associated with naturally occurring synapse elimination. *Neuron* **37**, 67–73 (2003).
7. Tom, V.J., Steinmetz, M.P., Miller, J.H., Doller C.M. & Silver J. Studies on the development and behavior of the dystrophic growth cone, the hallmark of regeneration failure, in an *in vitro* model of the glial scar and after spinal cord injury. *J. Neurosci.* **24**, 6531–6539 (2004)
8. Firkins, S.S., Bates, C.A., & Stelzner, D.J. Corticospinal tract plasticity and astroglial reactivity after cervical spinal injury in the postnatal rat. *Exp. Neurol.* **120**, 1–15 (1993).
9. Demjen, D. *et al.* Neutralization of CD95 ligand promotes regeneration and functional recovery after spinal cord injury. *Nat. Med.* **10**, 389–395 (2004).
10. Houle, J.D. & Jin, Y. Chronically injured supraspinal neurons exhibit only modest axonal dieback in response to a cervical hemisection lesion. *Exp. Neurol.* **169**, 208–217 (2001).
11. Perry, V.H., Brown, M.C., & Lunn, E.R. Very slow retrograde and Wallerian degeneration in the CNS of C57BL/Ola mice. *Eur. J. Neurosci.* **3**, 102–105 (1991).
12. Mack, T.G. *et al.* Wallerian degeneration of injured axons and synapses is delayed by a Ube4b/Nmnat chimeric gene. *Nat. Neurosci.* **4**, 1199–1206 (2001).
13. George, E.B., Glass, J.D. & Griffin, J.W. Axotomy-induced axonal degeneration is mediated by calcium influx through ion-specific channels. *J. Neurosci.* **15**, 6445–6452 (1995).
14. Zhai, Q. *et al.* Involvement of the ubiquitin-proteasome system in the early stages of Wallerian degeneration. *Neuron* **39**, 217–225 (2003).
15. Saido, T.C. *et al.* Spatial resolution of fodrin proteolysis in postischemic brain. *J. Biol. Chem.* **268**, 25239–25243 (1993).
16. Hill, C.E., Beattie, M.S. & Bresnahan, J.C. Degeneration and sprouting of identified descending supraspinal axons after contusive spinal cord injury in the rat. *Exp. Neurol.* **171**, 153–169 (2001).
17. Li, Y. & Raisman, G. Sprouts from cut corticospinal axons persist in the presence of astrocytic scarring in long-term lesions of the adult rat spinal cord. *Exp. Neurol.* **134**, 102–111 (1995).
18. Pan, Y.A., Misgeld, T., Lichtman J.W. & Sanes, J.R. Effects of neurotoxic and neuroprotective agents on peripheral nerve regeneration assayed by time-lapse imaging *in vivo*. *J. Neurosci.* **23**, 11479–11488 (2003)
19. Raff, M.C., Whitmore, A.V. & Finn, J.T. Axonal self-destruction and neurodegeneration. *Science* **296**, 868–871 (2002).
20. Bareyre, F.M. *et al.* The injured spinal cord spontaneously forms a new intraspinal circuit in adult rats. *Nat. Neurosci.* **7**, 269–277 (2004).
21. Nguyen, Q.T., Sanes, J.R. & Lichtman, J.W. Pre-existing pathways promote precise projection patterns. *Nat. Neurosci.* **5**, 861–867 (2002).
22. Beirowski, B. *et al.* Quantitative and qualitative analysis of Wallerian degeneration using restricted axonal labelling in YFP-H mice. *J. Neurosci. Meth.* **134**, 23–35 (2004).
23. Gillingwater, T.H. *et al.* Age-dependent synapse withdrawal at axotomised neuromuscular junctions in Wld(s) mutant and Ube4b/Nmnat transgenic mice. *J. Physiol.* **543**, 739–755 (2002).